



Article

A Robust Protocol for Entropy Measurement in Mesoscopic Circuits

Timothy Child^{1,2,*} , Owen Sheekey^{1,2}, Silvia Lüscher^{1,2,*}, Saeed Fallahi^{3,4,5}, Geoffrey C. Gardner^{4,5,6}, Michael Manfra^{3,4,5,6,7} and Joshua Folk^{1,2,*} 

¹ Stewart Blusson Quantum Matter Institute, University of British Columbia, Vancouver, BC V6T 1Z4, Canada; oisheekey@gmail.com

² Department of Physics and Astronomy, University of British Columbia, Vancouver, BC V6T 1Z1, Canada

³ Department of Physics and Astronomy, Purdue University, West Lafayette, IN 47907, USA; sfallahi@purdue.edu (S.F.); mmanfra@purdue.edu (M.M.)

⁴ Birck Nanotechnology Center, Purdue University, West Lafayette, IN 47907, USA; geoff@purdue.edu

⁵ Microsoft Quantum Lab Purdue, Purdue University, West Lafayette, IN 47907, USA

⁶ School of Materials Engineering, Purdue University, West Lafayette, IN 47907, USA

⁷ School of Electrical and Computer Engineering, Purdue University, West Lafayette, IN 47907, USA

* Correspondence: timjchild@phas.ubc.ca (T.C.); luescher@physics.ubc.ca (S.L.); jfolk@physics.ubc.ca (J.F.)

Abstract: Previous measurements utilizing Maxwell relations to measure change in entropy, S , demonstrated remarkable accuracy in measuring the spin-1/2 entropy of electrons in a weakly coupled quantum dot. However, these previous measurements relied upon prior knowledge of the charge transition lineshape. This had the benefit of making the quantitative determination of entropy independent of scale factors in the measurement itself but at the cost of limiting the applicability of the approach to simple systems. To measure the entropy of more exotic mesoscopic systems, a more flexible analysis technique may be employed; however, doing so requires a precise calibration of the measurement. Here, we give details on the necessary improvements made to the original experimental approach and highlight some of the common challenges (along with strategies to overcome them) that other groups may face when attempting this type of measurement.

Keywords: thermodynamic entropy; quantum dot; metrology; mesoscopic device



Citation: Child, T.; Sheekey, O.; Lüscher, S.; Fallahi, S.; Gardner, G.C.; Manfra, M.; Folk, J. A Robust Protocol for Entropy Measurement in Mesoscopic Circuits. *Entropy* **2022**, *24*, 417. <https://doi.org/10.3390/e24030417>

Academic Editor: Armin Feldhoff

Received: 24 February 2022

Accepted: 13 March 2022

Published: 17 March 2022

Publisher's Note: MDPI stays neutral with regard to jurisdictional claims in published maps and institutional affiliations.



Copyright: © 2022 by the authors. Licensee MDPI, Basel, Switzerland. This article is an open access article distributed under the terms and conditions of the Creative Commons Attribution (CC BY) license (<https://creativecommons.org/licenses/by/4.0/>).

1. Introduction

Direct measurements of entropy in nanoscale systems have the potential to identify and explore exotic quantum states that are otherwise difficult to distinguish from more conventional quantum states. Although entropy, S , is a common metric in macroscopic systems obtained through the measurement of the heat capacity of the system, this quantity is immeasurably small for nano-scale quantum systems and requires a different approach entirely. Strategies have been proposed for quantifying entropy based on electronic measurements of conductance, thermopower, or charge detection, each of which can provide easily detectable signals, even in the smallest of quantum devices [1–6]. Comparing the three approaches, strategies based on conductance and thermopower can typically be performed closer to equilibrium but are more limiting in the coupling required between mesoscopic circuit and leads.

Here, we focus on the third approach, using Maxwell relations to measure S (or, more accurately, changes in S) by sensing changes in charge with temperature. Recently, Ref. [1] followed the charge-sensing approach to measure ΔS associated with the addition of a single spin-1/2 electron in a lithographically defined quantum dot. This experiment served as a promising step toward a direct entropy measurement protocol based on charge sensing. Unfortunately, the precise implementation of the Maxwell relation in that initial work limited its applicability to relatively simple systems for which the measurement of entropy

holds little scientific value and allowed only the determination of entropy change caused by adding one full electron at a time. At the same time, the experimental method described in that work left room for artifacts in the measurement signal that could contaminate the determination of ΔS .

The goal of this paper is to outline the improvements made to the experimental approach in Ref. [1] that make it more robust at a technical level and applicable to a broader range of measurements. From the analytical side, the extraction of ΔS is based on a different formulation of the Maxwell relation [7],

$$\Delta S_{\mu_1 \rightarrow \mu_2} = \int_{\mu_1}^{\mu_2} \frac{dN(\mu)}{dT} d\mu, \quad (1)$$

where N represents the occupation of the quantum dot (QD), and T and μ are the temperature and chemical potential of the electron reservoir, respectively. Equation (1) enables the determination of entropy (change) continuously as a function of gate voltages or other parameters that control μ . In the experiment, significant improvements to the thermal design and measurement protocol eliminate many sources of error. Beyond the description of the new experimental protocol, we describe common challenges and possible strategies to overcome them that other groups may encounter in attempting this type of measurement.

2. Device Design and Layout

A circuit designed to measure the entropy of a QD using $\partial S/\partial\mu = \partial N/\partial T$ must have three elements: a QD coupled to an electron reservoir with a tunable chemical potential μ , the ability to change the temperature of this reservoir, and a charge sensor to detect the occupation of the QD. At the outset, it is important to note that μ referred to in the Maxwell relation is the chemical potential of the thermodynamic reservoir, which cannot easily be controlled in the experiment [3]. Instead, we tune the energy of the QD level, that is, the energy required to add an additional electron to the dot. In practice, it is the difference between μ and the QD energy that controls when electrons will enter the dot, so tuning the dot level effectively tunes μ as it appears in Equation (1).

Figure 1 shows an example of a circuit with the three elements listed above; it is identical to the circuit reported in Ref. [8] and similar in functionality to the one described in Ref. [1]. The circuit was defined using electrostatic gates on a GaAs/AlGaAs heterostructure, following a standard nanolithography process laid out in Ref. [8]. Measurements were carried out in a dilution refrigerator at temperatures ranging from 30 mK up to 500 mK. Electron temperatures below 30 mK were not attainable in our cryostat, and temperatures higher than 500 mK brought in sources of S unrelated to those of interest in the measurement.

The QD itself was defined following standard design guidelines developed through two decades of few-electron dot measurements across the mesoscopics community; see, for example, Refs. [9–11]. The gates immediately surrounding the dot were cooled down with a +400 mV bias so that when cold, the 2DEG under the gates was depleted of carriers with no voltage applied. The resulting QD could be readily tuned to an occupation of $0 \rightarrow \sim 5+$ electrons using the surrounding gates, with V_p dedicated to coarse tuning of the dot occupation.

Two advantages of a charge-sensing measurement that simplifies device design are that the entropy detection protocol itself is relatively insensitive to coupling through the QD tunnel barrier and that only one such barrier is required. However, some factors are especially important for the entropy measurement that may not be as relevant in other experiments. For example, tuning of the chemical potential (QD energy level) is central to this technique, and this tuning must be accomplished without changing other dot parameters significantly. For this reason, the design includes a gate extending into the middle of the dot, labeled V_D in Figure 1, with a very large electrostatic coupling to the QD electron wavefunction: the lever arm of this gate (the ratio of the change in QD energy to

the gate voltage applied) was typically 0.2 eV/V for this gate, compared with 0.04 eV/V or less for V_P .

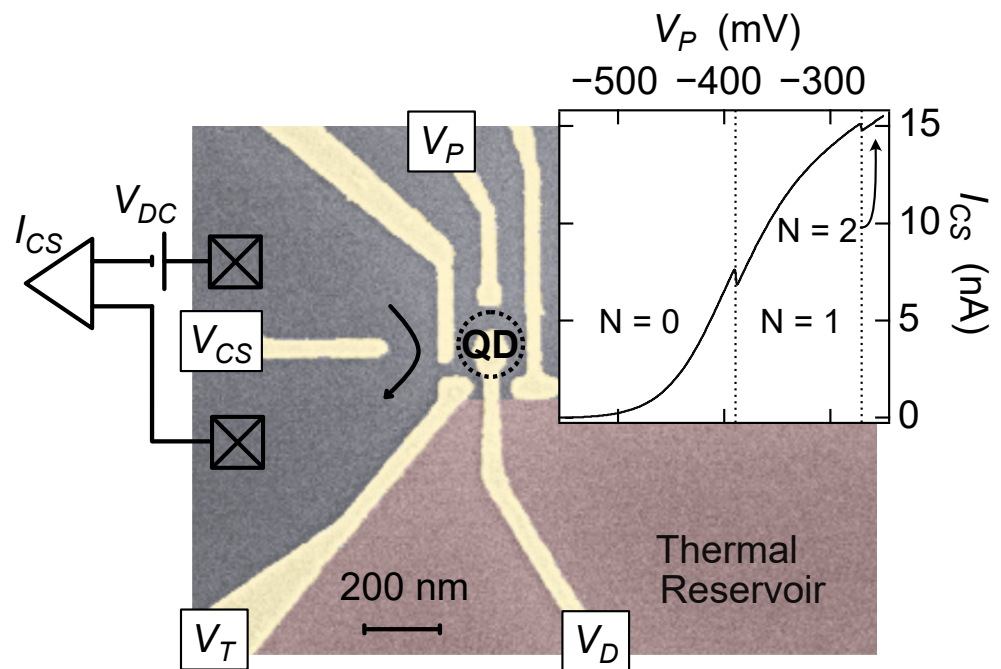


Figure 1. (main panel) False colored scanning electron micrograph (SEM) of the key parts of the entropy sensor. Electrostatic gates (gold) define the circuit in a 2D electron gas (2DEG). The thermal electron reservoir (red) can be rapidly heated by driving current through quantum point contacts (QPCs) far away. (inset) Current through the charge sensor, I_{CS} , for a wide sweep of the coarse plunger gate, V_P , demonstrating the alignment of the $0 \rightarrow 1$ transition at the steepest part of the trace to maximize sensitivity.

The quantum point contact (QPC) operated as a charge sensor (CS) was formed by the three leftmost gates in Figure 1, and used to detect the occupation of the QD [12–14]. A DC bias, typically between 50 and 300 μV , was applied across the CS, with the resulting current I_{CS} recorded using a current–voltage converter (10^8 A/V, 1 kHz bandwidth set by a two-stage low-pass filter). For the measurement protocol described here, real-time monitoring of the current is important, so the output of the current preamplifier was fed into an analog–digital converter with a 2.5 kHz sample rate.

V_{CS} was tuned to maximize the CS sensitivity to charge in the QD. The inset to Figure 1 shows $0 \rightarrow 1 \rightarrow 2$ electron transitions for the QD, in this case driven by V_P , with the $0 \rightarrow 1$ transition tuned to the steepest slope below the 1st conductance plateau. The relatively large cross capacitance between V_P and the CS is apparent in the data in Figure 1 inset: just 200 mV applied to V_P can tune the QPC from pinch-off nearly to full transmission. This highlights the importance of tuning dot occupation with V_D during the entropy measurement.

The CS sensitivity could also be increased by tuning the gates around the dot to bring the center of the electron wavefunction as close as possible to the CS: in some cases, we were able to achieve a 10% change in CS transmission due to the addition of an electron to the QD, using this gate geometry. We point out, however, that increasing the QD–CS coupling has both advantages and disadvantages. Stronger coupling reduces the bias that must be applied to the CS for the same signal to noise. At the same time, stronger coupling shifts the charge detection process farther from the weak measurement limit that may be desirable from the point of view of back-action on the quantum system under study [15–17]. Which of these factors is more important will, in general, be different from experiment to experiment.

The coupling of the QD to the heated electron reservoir was controlled by V_T . For simplicity, the measurements presented here are in the weak coupling limit (very negative V_T), where broadening of the QD energy levels due to the coupling with the reservoir, Γ , is much less than that of thermal broadening ($\Gamma \ll k_B T$); however, measurements using this technique are also possible in the strongly coupled regime [8]. For the measurements presented here, Γ is estimated to be of the order $0.001 k_B T$ (extrapolated from measurements in the strong coupling regime where Γ measurably broadens the charge transition [8]). The limit on arbitrarily weak coupling arises from the requirement that the tunneling rate between the QD and the reservoir must be much faster than the measurement rate (the inverse of the time spent sitting at each setting of μ during which an average N was recorded). From a thermodynamic perspective, this restriction ensures that the QD can transition between all available microstates within the measurement time.

3. Measurement Protocol

The measurement of $\partial N/\partial T$ that is central to Equation (1) was carried out by evaluating the discrete derivative $\Delta N/\Delta T$, using the CS to monitor the change in N between two nearby temperatures $\Delta N = (N(T + \Delta T) - N(T))$. The choice to measure at two particular values of T , rather than the simpler approach of oscillating T (approximately) sinusoidally at frequency f_T , then locking into variations in N at f_T , was found to be important to the quantitative determination of ∂T in Equation (1) with better than 10–20% error, and was also helpful in troubleshooting spurious changes in the dot potentials that could appear when attempting to change only T .

It is the response of N to temperature alone, with all other parameters (such as μ) constant, that contains information about the entropy of the system. This requirement, for identical μ between the two temperatures, turns out to pose a significant experimental challenge. In practice, any changes $\delta\mu$ in the dot energy between the measurements at $T + \Delta T$ and T will introduce inaccuracy in the entropy measurement by an amount of order $\delta\mu/(k_B \Delta T)$. For measurements below 100 mK, where ΔT is less than a few tens of mK, this restricts $\delta\mu$ between the two temperatures to be much less than 1 μeV for an accurate determination of ΔS . There are both intrinsic and extrinsic factors that must be taken into account in order to keep μ constant to such a high degree.

Quantum dots fabricated in GaAs/AlGaAs heterostructures experience intrinsic, albeit small, electrostatic fluctuations due to nearby charge motion in the dopant layer of the heterostructure, resulting in noise in the QD energy with a frequency spectrum typically between $1/f$ and $1/f^2$ [18,19]. It is therefore crucial that the measurements $N(T + \Delta T)$ and $N(T)$ be carried out as close to each other in time as possible, protecting the measurement from noise in the low- f limit. The requirement to alternate rapidly between hot and cold reservoir temperatures mandates that the temperature change is accomplished locally on the chip, rather than by changing the temperature T of the entire cryostat. For this reason, and to minimize the heat capacity of the thermal system, Joule heating due to a bias current I_H was used to raise the electron temperature T_e of the thermal reservoir adjacent to the QD (Figure 1) above the sample (chip) temperature T : $T_e = T$ when $I_H = 0$ and $T_e = T + \Delta T$ at finite I_H .

Driving I_H directly into the thermal reservoir will generally change its potential, however. Since μ is defined with respect to the chemical potential of the reservoir, this direct effect of I_H must be avoided. At the same time, the advantage of very local heating must be balanced by the requirement for full thermal equilibration of charge carriers in the reservoir, in contrast to the non-equilibrium distribution that is expected when injecting carriers at high bias through a mesoscopic circuit.

A two-chamber heater was used to ensure a thermalized electron reservoir with a μ that did not change when the Joule heating current was applied (Figure 2a): I_H was sourced through QPC1 and drained through QPC2 to heat the first chamber directly, whereas the second chamber (the thermal reservoir immediately adjacent to the QD) was heated indirectly by electrons diffusing from the first chamber through QPC3. Cooling of the

reservoirs occurred via electron–phonon coupling (especially at higher temperatures) and by diffusion through QPC1, QPC2, and QPC4 to the 2DEG regions connected to ohmic contacts, which remain at the chip temperature due to their large volume and therefore strong electron–phonon equilibration. For most experiments, QPCs 1, 2, and 3 were set at their $2e^2/h$ conductance plateau, while QPC4 was set at $6e^2/h$.

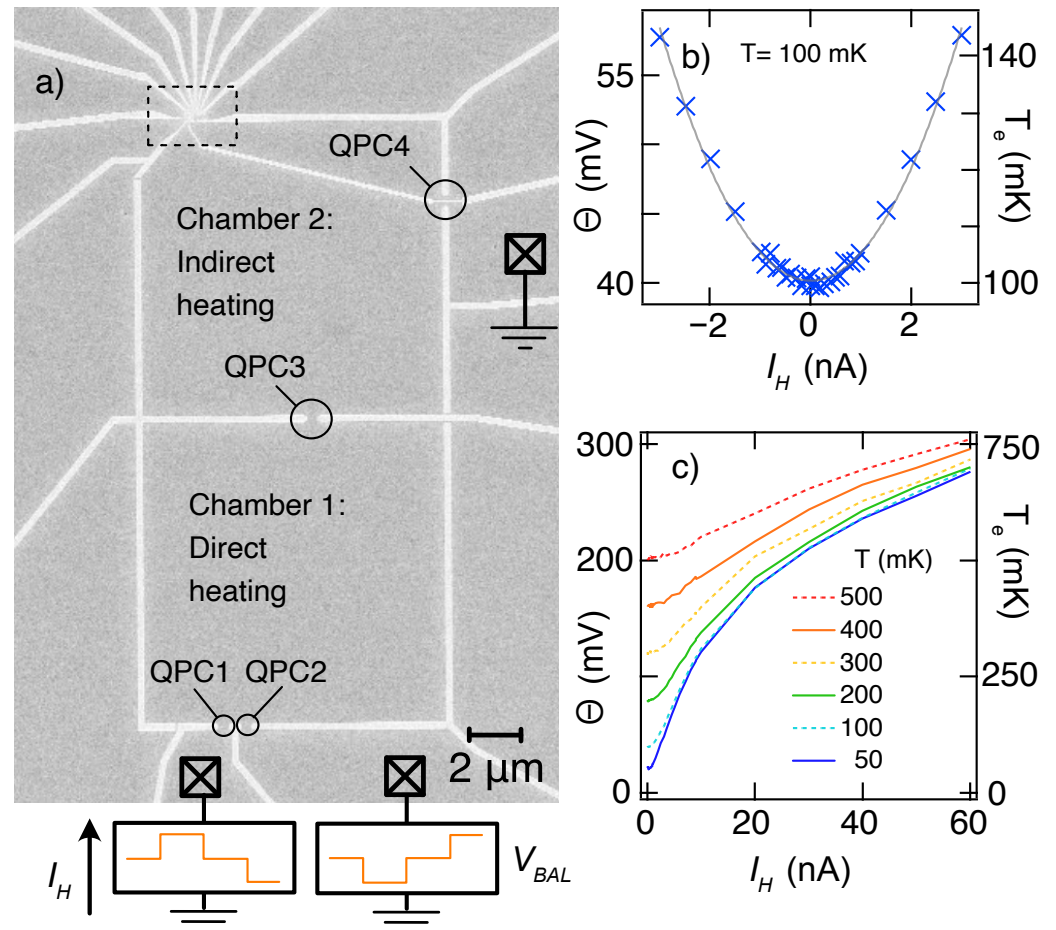


Figure 2. (a) SEM micrograph of the full measurement device showing the large ($10\ \mu\text{m}$ square) chambers used for electron thermalization, QPCs 1 and 2 through which Joule heating current I_H flowed, and QPCs 3 and 4 through which heat diffused but no net current flowed. The dashed rectangle in the upper left is the region shown in Figure 1, including QD and charge sensor. (b) Crosses: broadening of the charge transition (Θ , left axis), converted to electron temperature (T_e , right axis), increases above the sample temperature, $T_s = 100\ \text{mK}$, due to I_{bias} driven through QPCs 1 and 2. Solid line: quadratic fit to $|I_H| < 1\ \text{nA}$ data, with deviations seen at higher $|I_H|$. (c) Extension of panel (b) to higher I_H and for a range of different sample temperatures. Sub-linear behavior at very large I_H reflects electron–phonon cooling at higher temperatures.

One advantage of using quasi-enclosed chambers for heating is the relatively low values of I_H required to achieve a significant temperature rise. Figure 2b shows that T_e of chamber 2, measured via the broadening of a weakly coupled charge transition in the QD, can be increased from a sample temperature $T = 100\ \text{mK}$, to $T + \Delta T \sim 130\ \text{mK}$, with I_H less than $2.5\ \text{nA}$. At a quantitative level, of course, the temperature rise for a given current depends on the settings of all four QPCs.

The electron temperature is approximately quadratic in I_H for small heating currents, as might be expected from Joule heating power $P \propto I_H^2$, but already by $\Delta T \sim 20\ \text{mK}$ small deviations are visible in Figure 2b, where $T = 100\ \text{mK}$. The deviations become more extreme at higher I_H or lower chip temperature T . Non-quadratic behavior results from the

temperature dependence of the thermal conductivity κ between the reservoir electrons and the cold thermal ground, whether it be via electron–phonon coupling to the chip’s lattice ($\kappa_{e-ph} \propto T^{3-4}$ expected) or Wiedemann–Franz cooling ($\kappa_{WF} \propto T$ expected) to the cold reservoirs connected to ohmic contacts [20]. Figure 2c illustrates the extreme deviation from quadratic behavior for large I_H , corresponding to large ΔT . The sub-linear lineshape of $T_e(I_H)$ at the highest currents demonstrates that phonon cooling has become dominant. It is worth noting that the deviation from $\Delta T \propto I_H^2$ makes the lock-in-based approach, which relies on T_e changing at the second harmonic of a sinusoidal I_H , especially challenging to calibrate accurately and provides further support for the discrete alternation between T and $T + \Delta T$ used here.

The potential of chamber 2 (Figure 2a) was held constant by biasing I_H through QPC1 while applying a balancing voltage V_{BAL} behind QPC2. V_{BAL} was tuned such that the potential in chamber 2, when sensed directly by the QD, remained constant. The inverse signs of I_H into QPC1 and V_{BAL} behind QPC2 are illustrated schematically at the bottom of Figure 2a. In order to alternate the temperature while ensuring that μ stays constant, opposing three-level square waves were created by two channels of a 2.5 kHz digital–analog converter to generate I_H and V_{BAL} . The top row of Figure 3 shows the square wave driving I_H , with an inverse wave setting V_{BAL} . The square wave has four 20 ms segments: two segments heated with equal magnitude but opposite sign ($I_H = \pm 3$ nA in this case), separated by two segments at $I_H = 0$. Only after confirming the expected response in all four segments is it possible to conclude that the heating process has not affected μ .

Figure 3a–d show the response of the charge sensor (I_{CS}) to the square wave, at the four positions along the charge transition indicated by arrows in Figure 3e. Before and after the transition (Figure 3a,d) there is no effect of I_H . Checking these “control” positions is important to confirm the absence of spurious coupling between I_H and the charge sensor, such as capacitive coupling between the wires carrying I_H and those carrying I_{CS} , or between the current path of I_H and the charge sensor itself. Before the midpoint of the transition (Figure 3b), Joule heating of chamber 2 leads to a drop in I_{CS} , reflecting extra charge in the dot and therefore positive dN/dT (Equation (1)). Within the noise of this measurement, there is no difference between positive and negative I_H . This confirms that first-order effects of I_H are strongly suppressed, for example by properly setting V_{BAL} . For $V_D \gtrsim 0.03$ mV, the dN/dT changes sign before returning to zero well past the transition.

The raw data, $I_{CS}(t)$, are processed to determine a single value ΔI_{CS} for each V_D . This involves separating the data into two segments corresponding either to T or $T + \Delta T$. Before that is done, however, it is important to remove the time periods during which the measurement is settling to new parameter values. This settling time, on the order of a few microseconds, is clearly visible in Figure 3b,c. We note that the rate of settling is limited by the response of the cryostat wiring in our case; thermal equilibration times within the device are many orders of magnitude faster. The two segments at T , or $T + \Delta T$, are then averaged to find $I_{CS}(T)$, or $I_{CS}(T + \Delta T)$. These values, determined at each V_D , are plotted in Figure 3e in blue (T) and red ($T + \Delta T$), with the difference, ΔI_{CS} , in Figure 3f.

$\Delta N/\Delta T$ is obtained from the ΔI_{CS} measurement using parameters obtained from the charge transition itself, $I_{CS}(V_D)$. Weakly coupled transitions are broadened by the Fermi–Dirac distribution in the reservoir and may be fit to [21,22]

$$I_{CS}(V_D) = \frac{-I_e}{2} \tanh\left(\frac{V_D - V_0}{2\Theta}\right) + I'(V_D - V_0) + I_0, \quad (2)$$

where I_e quantifies the sensitivity of the charge sensor to the occupation of the QD, V_0 is the center of the charge transition, Θ represents the thermal broadening in equivalent gate voltage, I' quantifies the cross-capacitance between V_D and the CS, and I_0 is the current through the charge sensor midway through the transition. Although the cross-capacitance is well approximated as a simple linear term for weakly coupled transitions, for more strongly coupled transitions, it may have different slopes on the $N = 0$ and $N = 1$ sides of the transition, which require more elaborate fitting.

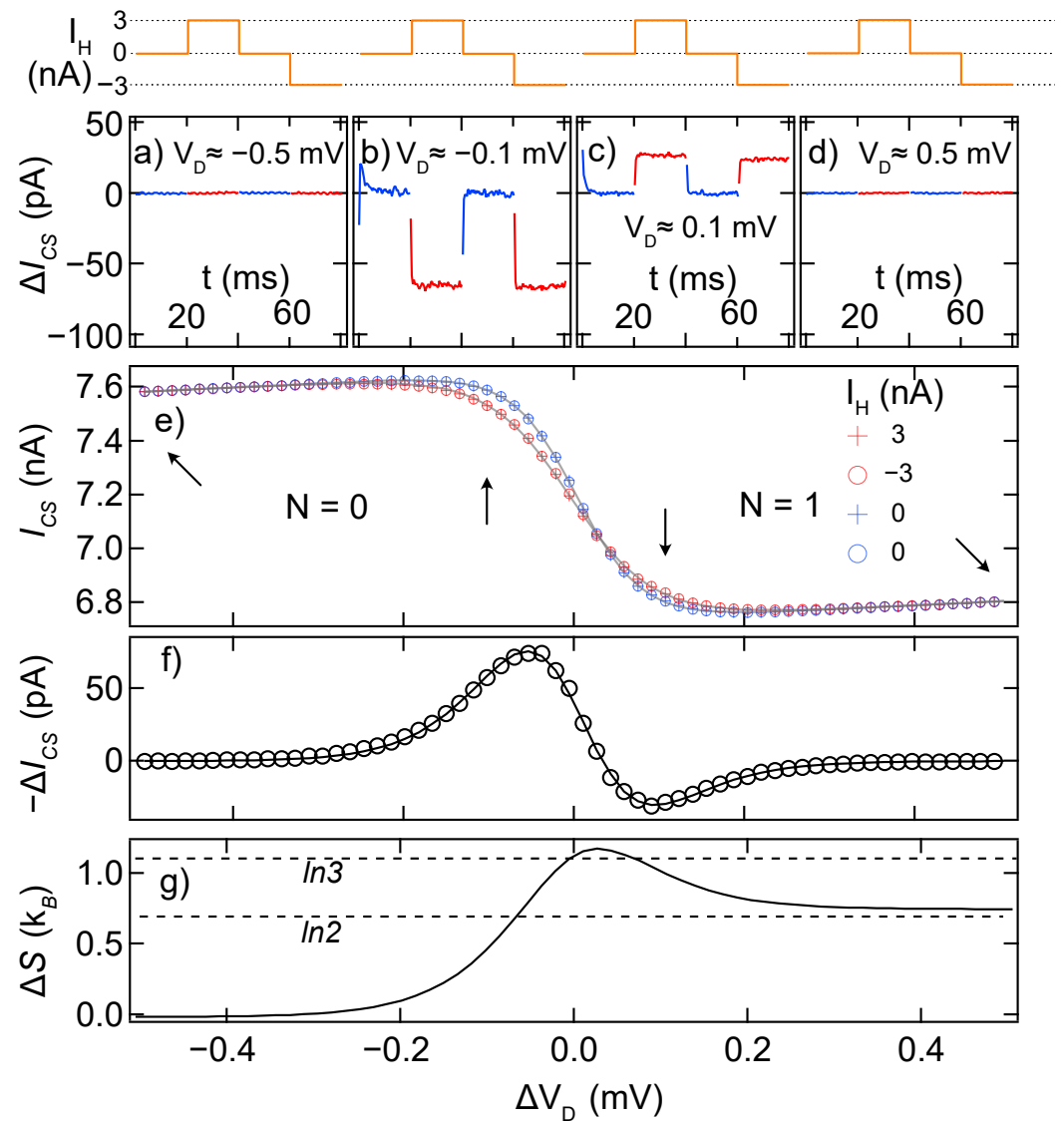


Figure 3. A step-by-step inspection of the analysis procedure that goes into an eventual calculation of ΔS . The fine-tuning plunger gate, V_D , is used to lower the energy of the QD level such that one electron enters from the thermal reservoir. (top) Schematic illustration of $I_H(t)$ through one complete 80 ms cycle. (a–d) Charge sensor current through the 80 ms cycle, calculated with respect to the unheated sections, at four locations on the $0 \rightarrow 1$ transition: $V_D = -0.5, -0.1, 0.1, 0.5$ mV. Data shown here are averaged over 1200 square wave cycles. Blue (red) indicates times at which the thermal reservoir is unheated (heated). The relaxation time of the measurement (~ 3 ms) is visible in panels (b,c). (e) Charge sensor current separated into averages over the 4 parts of the square heating wave, where heating is applied with an alternating current direction ($I_H = 3, -3$ nA), with zero bias applied in between ($I_H = 0$). Fits to the average “cold” and “hot” data are shown in grey. (f) The difference in charge sensor current between the “cold” and “hot” traces. (g) $\Delta S(V_D)$ obtained by integration of ΔI_{CS} using Equation (1). ΔT is 28.1 mK, equivalent to 0.011 mV when converted to effective gate voltage, determined from the difference in thermal broadening of heated and unheated I_{CS} .

Of these parameters, I_e and Θ are crucial to the conversion between ΔI_{CS} and $\Delta N / \Delta T$. I_e is the difference in current through the charge sensor between the unoccupied ($N = 0$) and occupied ($N = 1$) states, and is therefore used to scale the charge sensor reading to $\Delta N = -\Delta I_{CS} / I_e$ (the minus sign appears because an increase in N causes a drop in I_{CS}). ΔT is determined from the difference in the broadening term, Θ , for heated and unheated

transitions. This calculation is straightforward when the QD is in the weakly coupled limit, with the charge transition well modeled by Equation (2). As determined by fits to Equation (2), Θ will have units of gate voltage instead of energy, and the lever arm $\alpha \equiv \Delta\epsilon/\Delta V_D$ that converts changes in the gate voltage V_D to changes in the dot energy ϵ would be needed to convert Θ to $k_B T$. In practice, it is more convenient to perform the integral in Equation (1) over the gate voltage V_D actually controlled in the measurement, rather than over the equivalent μ (in units of energy). Therefore, the denominator in the integrand $\Delta N/\Delta T$ is more conveniently expressed as $\Delta\Theta$ in units of equivalent V_D rather than ΔT in Kelvin. The ΔS obtained (Figure 3g) by this approach is then in units of k_B . Following this procedure, the factor α cancels and needs not be measured directly.

For the addition of an electron to a weakly coupled non-interacting QD, the expected entropy change throughout the transition is well modeled by the classical Gibbs entropy, $S = -k_B \sum p_i \ln p_i$, and is effectively the combination of charge degeneracy (electron in/out of QD) and spin degeneracy (electron spin-up/down) of the QD. Note that the measurements in Figure 3 start with the QD in an unoccupied state ($S = k_B \ln 1 = 0$); as a result, the ΔS measurement (Figure 3) is equal to the total S of the QD. When the lowest energy level of the QD is brought closer to μ by more positive V_D , the average occupation of the QD begins to increase from zero (at $V_D \sim -0.3$ mV). The additional possible states for the QD to be in (occupied spin-up/down) results in the entropy of QD increasing, until the QD is on average two thirds occupied ($N = 2/3$). At this point, the three possible states of the QD—unoccupied, spin-up, or spin-down—are each equally probable and, hence, the expected $S = \Delta S = k_B \ln 3$. As the QD tends toward unitary average occupation, the system is no longer charge degenerate, resulting in a final state where only the spin degeneracy of the occupied state is left and, hence, the expected $S = \Delta S = k_B \ln 2$. The values $1.07 k_B \ln 3$ and $1.07 k_B \ln 2$ in Figure 3g illustrate typical experimental errors resulting from the approach outlined in this paper. It is more robust in the sense that this technique can be applied to arbitrarily complex systems without modification to the analysis procedure; however, it is susceptible to calibration errors, giving a typical uncertainty of up to 10% for this method.

4. Common Problems

The rather complicated thermalization device design described in the previous section was arrived at after an initial round of experiments, e.g., Ref. [1], with a much simpler design. That design is illustrated in Figure 4, with Joule heating through a single QPC directly across a channel from the QD to be measured. In addition to the more efficient heating in the present design ($\Delta T \sim 30$ mK at $T = 100$ mK requires 3 nA at 40 μ V bias compared to 8 nA at 160 μ V bias in Ref. [1]), Figure 4b,c illustrates two of the experimental artifacts that were introduced by the simpler design.

Figure 4b shows the effect of poor thermalization of the electrons due to I_H before they interact with the dot. Electrons (or holes) passing through the Joule heating QPC enter the reservoir (channel) with very high energy (160 μ eV in the example above) compared to the final temperature they will have after equilibration ($k_B \cdot 130$ mK ~ 11 μ eV). Due to the ballistic nature of the channel (mean free path > 5 μ m), the electrons will impinge on the QD far from equilibrium when arriving due to a straight path trajectory [23]. The effect of this non-equilibration is visible in the ΔI_{CS} data taken with transverse field $B_{\perp} = 0$, as a series of bumps preceding the peak in ΔI_{CS} , deviating dramatically from the theoretical curve shown with a solid line. Although we do not have a microscopic explanation for the details of these bumps, they are suppressed by B_{\perp} as the trajectories from heating QPC are bent away from the QD. Unfortunately, magnetic fields of at least 200 mT were required to eliminate these deviations entirely (Figure 4b), and at this field, the entropy measurement was perturbed both by the Zeeman energy of the field and by the onset of Shubnikov de Haas oscillations in the channel.

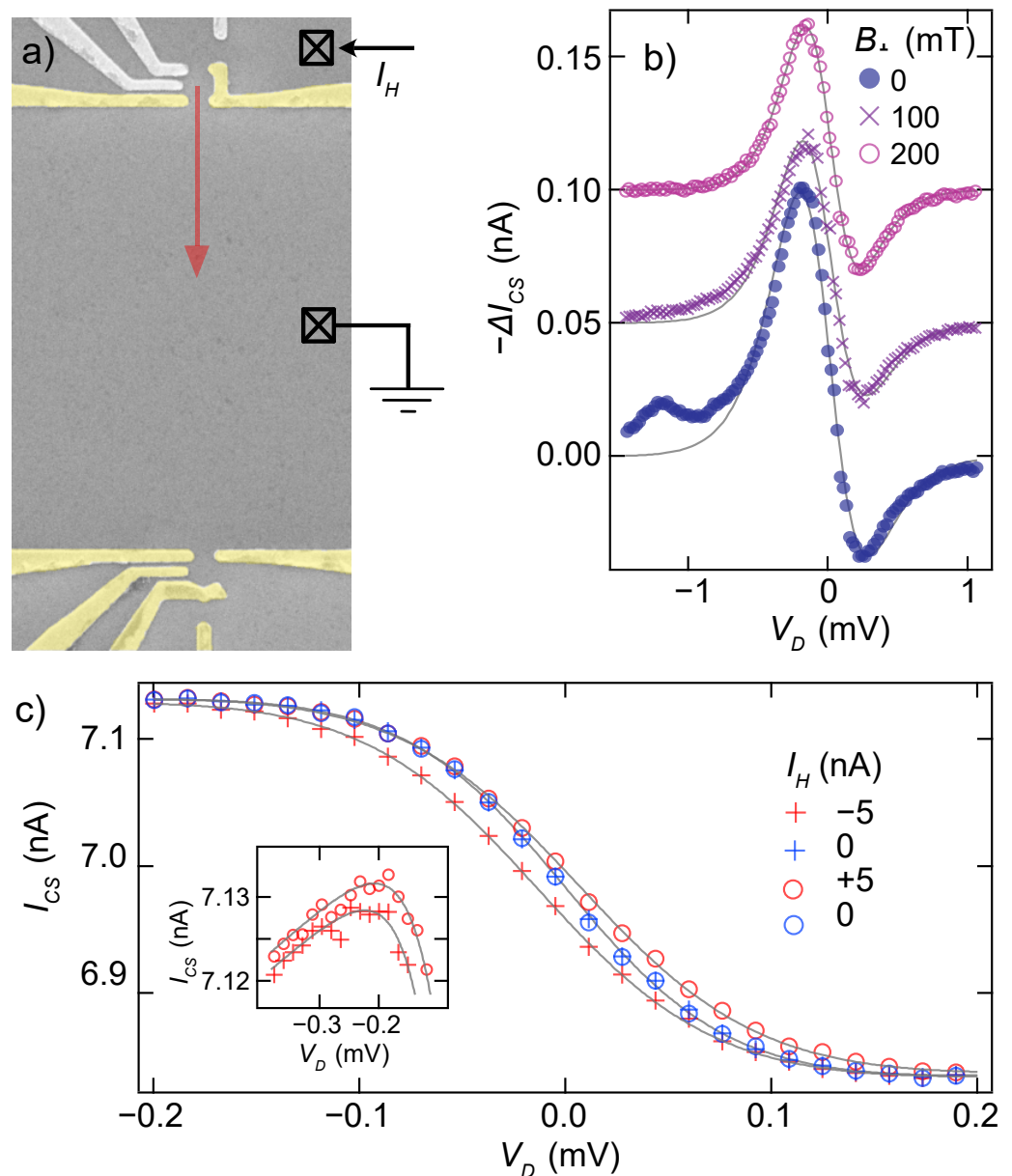


Figure 4. (a) False-color scanning electron micrograph similar to the entropy measuring circuit from Ref. [1] where the thermal electron reservoir was heated by I_H through a single QPC (top), with no additional confinement of the heated channel. (b) Using the circuit in panel (a), ΔI_{CS} measurements over the $0 \rightarrow 1$ transition for 0, 100 and 200 mT of magnetic field applied perpendicular to the plane of the 2DEG. Then, 100 and 200 mT data are offset by 0.05 and 0.1 nA respectively. Illustrates the effect of unthermalized electrons from the heater QPC reaching the QD, for 0 and 100 mT data. Fits to theory for weakly coupled transitions (solid grey) emphasize the deviation of data from theory on the $N = 0$ side of the transition. (c) Four segments of I_H square wave averaged separately, analogous to Figure 3e and made using the circuit in Figure 2a, but without proper balancing to keep the chemical potential of the reservoir at ground. The result is a shift of $I_H = +5$ nA with respect to -5 nA data. Inset: zoom-in to the $V_D = -0.4 \rightarrow -0.1$ mV range of the main panel, showing both lateral and vertical offsets ± 5 nA data.

Figure 4c illustrates the damaging effect of the direct (linear) offset of the reservoir potential due to I_H . When I_H is driven through the heater QPC in the geometry from Figure 4a, a voltage offset is generated in the reservoir outside the QD due to the non-zero resistance to ground. This offsets μ in Equation (1), contravening the requirement to measure $\partial N/\partial T$ with μ fixed. At the same time, it may have a capacitive effect on the

charge sensor, directly affecting the measurement of N . Because these effects reverse with the sign of the current being driven through the heater QPC, whereas the Joule heating itself does not, it is easy to identify their influence via a shift of the two heated traces (one at $+I_H$ and one at $-I_H$) away from each other. Direct influence on the reservoir potential causes the traces to separate laterally (Figure 4c main panel), whereas cross-capacitive effects on the charge sensor cause the traces to separate vertically (Figure 4c inset). Averaging the $\pm I_H$ traces together is not sufficient to remove these offsets due to non-linearity in $I_{CS}(V_D)$, and may artificially raise or lower the apparent entropy determined from analyzing ΔI_{CS} data.

5. Outlook

We described an improvement in the thermal circuit design and measurement protocol for quantifying entropy of mesoscopic devices in the quantum limit, based on monitoring how the charge of the system changes with temperature using a Maxwell relation. To conclude, we offer a few guidelines for how this technique may be improved and made more broadly applicable in the future.

Extending these measurements to new regimes with higher bandwidth measurements will immediately offer rewards in noise performance. The damaging effect of offset charge noise on quantum dot energy levels, which motivated the fast alternation between temperatures discussed in the Measurement Protocol section, is more severe in this type of experiment than in a typical mesoscopic investigation. The need to control μ at a sub- μeV level forces the measurement to be performed at as high a frequency as possible given the experimental setup, and fundamental speed limitations involving heat capacity of electrons are orders of magnitude above what was achieved in the present experiment.

Two more opportunities for improvement stem from the need to remain in thermal equilibrium in order for Maxwell relations to be applicable. The very act of charge sensing injects a non-equilibrium component into the system dynamics, in principle violating the starting requirement for Maxwell relations. This can be minimized by, first, reducing stray couplings between the sensor circuit and the device under test and, second, by reducing the noise of the charge sensing measurement itself. At the same time, the theoretical question of how much charge sensing is actually expected to affect dN/dT for a given system remains an important open avenue for study.

At a more mundane level, the requirement for operation in thermal equilibrium is hard to meet in complex circuits when following the electron heating approach outlined above. The advantage of heating only electrons is that the heat capacity is minuscule, and temperatures can change rapidly as a result. The disadvantage is that the electronic system is then out of thermal equilibrium with the phonon lattice, so parts of a multi-component mesoscopic circuit that couple differently to the heated electronic reservoir and to the phonon lattice may end up at different, and poorly defined, effective temperatures. This concern was not a factor in the proof-of-principle measurement of electron spin entropy laid out in Figure 1: the “system” (the electron in the dot) is easily brought into thermal equilibrium with the reservoir with even the weakest coupling between them because there are no internal degrees of freedom (within $k_B T$) for the first electron in a 200 nm diameter QD.

For more complex systems, with microstates spaced closely together (but not degenerate) in energy, the challenge will be greater. Future experiments may ultimately move away from this electron heating approach to a more intricate thermal circuit that maintains electrons and lattice phonons in thermal equilibrium during the heating step. This will require careful design, ensuring that thermal coupling between the chip and cryostat is strong enough to keep the chip close to the base temperature while the heating is off but weak enough to keep the chip in internal thermal equilibrium during the heating process [24].

There are numerous possibilities for measuring the entropy of interesting quantum systems using this technique (with adaptations to the heating procedure as discussed). Any system for which the ground state is modified by the occupation of the charge-sensed QD is a candidate—whether the QD is an integral part of the measured quantum

system, or whether the QD affects a nearby quantum system of interest purely through capacitive coupling. Considering the case of integral QDs, strongly coupling the QD to an electron reservoir could enable an entropy measurement in the presence of Kondo correlations [8]; alternatively, multi-dot systems (including the QD entropy probe) could simulate different regimes of the Hubbard model [25], such as the recent implementation of Nagaoka ferromagnetism [26]. Considering the case of remote QDs as probes of another system, the proposed detection of a Majorana fermion in Ref. [7]) is accomplished by tuning the Majorana–lead coupling electrostatically through the QD occupation.

Author Contributions: Conceptualization, T.C., O.S., S.L. and J.F.; methodology, T.C., O.S., S.L. and J.F.; software, T.C. and S.L.; formal analysis, T.C.; investigation, T.C. and O.S.; resources, S.F., G.C.G. and M.M.; writing—original draft preparation, T.C.; writing—review and editing, T.C., O.S., S.L. and J.F.; visualization, T.C. and O.S.; supervision, J.F.; project administration, J.F.; funding acquisition, M.M. and J.F. All authors have read and agreed to the published version of the manuscript.

Funding: This project has received funding from European Research Council (ERC) under the European Union’s Horizon 2020 research and innovation program under grant agreement No 951541, as well as from SBQMI, NSERC, CIFAR, and CFI. S.F., G.C.G. and M.M. were supported by the US DOE Office of Basic Energy Sciences, Division of Materials Sciences and Engineering award no. DE-SC0006671.

Data Availability Statement: All data and analysis presented in this manuscript can be found at [<https://github.com/TimChild/entropy-measurement-protocol>].

Acknowledgments: The authors acknowledge helpful conversations and important insights from Y. Meir, E. Sela and A. Mitchell. Experiments at UBC were undertaken with support from the Stewart Blusson Quantum Matter Institute, the Natural Sciences and Engineering Research Council of Canada, the Canada Foundation for Innovation, the Canadian Institute for Advanced Research, and the Canada First Research Excellence Fund, Quantum Materials and Future Technologies Program. Additional support from Nokia Bell Laboratories for the MBE facility at Purdue is gratefully acknowledged.

Conflicts of Interest: The authors declare no conflict of interest.

Abbreviations

The following abbreviations are used in this manuscript:

QD	Quantum Dot
CS	Charge Sensor
2DEG	Two-Dimensional Electron Gas
QPC	Quantum Point Contact
DC	Direct Current

References

- Hartman, N.; Olsen, C.; Lüscher, S.; Samani, M.; Fallahi, S.; Gardner, G.C.; Manfra, M.; Folk, J. Direct entropy measurement in a mesoscopic quantum system. *Nat. Phys.* **2018**, *14*, 1083–1086. [[CrossRef](#)]
- Kleeorin, Y.; Thierschmann, H.; Buhmann, H.; Georges, A.; Molenkamp, L.W.; Meir, Y. How to measure the entropy of a mesoscopic system via thermoelectric transport. *Nat. Commun.* **2019**, *10*, 5801. [[CrossRef](#)] [[PubMed](#)]
- Pyurbeeva, E.; Mol, J.A. A Thermodynamic Approach to Measuring Entropy in a Few-Electron Nanodevice. *Entropy* **2021**, *23*, 640. [[CrossRef](#)] [[PubMed](#)]
- Gehring, P.; Sowa, J.K.; Hsu, C.; de Bruijckere, J.; van der Star, M.; Le Roy, J.J.; Bogani, L.; Gauger, E.M.; van der Zant, H.S. Complete mapping of the thermoelectric properties of a single molecule. *Nat. Nanotechnol.* **2021**, *16*, 426–430. [[CrossRef](#)] [[PubMed](#)]
- Rozen, A.; Park, J.M.; Zondiner, U.; Cao, Y.; Rodan-Legrain, D.; Taniguchi, T.; Watanabe, K.; Oreg, Y.; Stern, A.; Berg, E.; et al. Entropic evidence for a Pomeranchuk effect in magic-angle graphene. *Nature* **2021**, *592*, 214–219. [[CrossRef](#)] [[PubMed](#)]
- Smirnov, S. Majorana ensembles with fractional entropy and conductance in nanoscopic systems. *Phys. Rev. B* **2021**, *104*, 205406. [[CrossRef](#)]
- Sela, E.; Oreg, Y.; Plugge, S.; Hartman, N.; Lüscher, S.; Folk, J. Detecting the universal fractional entropy of Majorana zero modes. *Phys. Rev. Lett.* **2019**, *123*, 147702. [[CrossRef](#)] [[PubMed](#)]

8. Child, T.; Sheekey, O.; Lüscher, S.; Fallahi, S.; Gardner, G.C.; Manfra, M.; Kleeorin, Y.; Meir, Y.; Folk, J. Entropy measurement of a strongly correlated quantum dot. *arXiv* **2021**, arXiv:2110.14158.
9. Elzerman, J.M.; Hanson, R.; Beveren, L.H.W.v.; Witkamp, B.; Vandersypen, L.M.K.; Kouwenhoven, L.P. Single-shot read-out of an individual electron spin in a quantum dot. *Nature* **2004**, *430*, 431–435. [[CrossRef](#)] [[PubMed](#)]
10. Hanson, R.; Kouwenhoven, L.P.; Petta, J.R.; Tarucha, S.; Vandersypen, L.M. Spins in few-electron quantum dots. *Rev. Mod. Phys.* **2007**, *79*, 1217. [[CrossRef](#)]
11. Barthel, C.; Kjærgaard, M.; Medford, J.; Stopa, M.; Marcus, C.M.; Hanson, M.P.; Gossard, A.C. Fast sensing of double-dot charge arrangement and spin state with a radio-frequency sensor quantum dot. *Phys. Rev. B* **2010**, *81*, 161308. [[CrossRef](#)]
12. Field, M.; Smith, C.G.; Pepper, M.; Ritchie, D.A.; Frost, J.E.F.; Jones, G.A.C.; Hasko, D.G. Measurements of Coulomb blockade with a noninvasive voltage probe. *Phys. Rev. Lett.* **1993**, *70*, 1311–1314. [[CrossRef](#)] [[PubMed](#)]
13. Sprinzak, D.; Ji, Y.; Heiblum, M.; Mahalu, D.; Shtrikman, H. Charge distribution in a Kondo-correlated quantum dot. *Phys. Rev. Lett.* **2002**, *88*, 176805. [[CrossRef](#)]
14. Elzerman, J.; Hanson, R.; Greidanus, J.; Van Beveren, L.W.; De Franceschi, S.; Vandersypen, L.; Tarucha, S.; Kouwenhoven, L. Few-electron quantum dot circuit with integrated charge read out. *Phys. Rev. B* **2003**, *67*, 161308. [[CrossRef](#)]
15. Aleiner, I.L.; Wingreen, N.S.; Meir, Y. Dephasing and the Orthogonality Catastrophe in Tunneling through a Quantum Dot: The “Which Path?” Interferometer. *Phys. Rev. Lett.* **1997**, *79*, 3740–3743. [[CrossRef](#)]
16. Silva, A.; Levit, S. Peculiarities of the controlled dephasing of a quantum dot in the Kondo regime. *EPL (Europhys. Lett.)* **2003**, *62*, 103. [[CrossRef](#)]
17. Kang, K.; Khym, G.L. Entanglement, measurement, and conditional evolution of the Kondo singlet interacting with a mesoscopic detector. *New J. Phys.* **2007**, *9*, 121. [[CrossRef](#)]
18. Buizert, C.; Koppens, F.H.L.; Piore-Ladrière, M.; Tranitz, H.P.; Vink, I.T.; Tarucha, S.; Wegscheider, W.; Vandersypen, L.M.K. In Situ Reduction of Charge Noise in GaAs/Al_xGa_{1-x}As Schottky-Gated Devices. *Phys. Rev. Lett.* **2008**, *101*, 226603. [[CrossRef](#)] [[PubMed](#)]
19. Liang, S.; Nakamura, J.; Gardner, G.; Manfra, M. Reduction of charge noise in shallow GaAs/AlGaAs heterostructures with insulated gates. *Appl. Phys. Lett.* **2020**, *117*, 133504. [[CrossRef](#)]
20. Mittal, A.; Wheeler, R.; Keller, M.; Prober, D.; Sacks, R. Electron-phonon scattering rates in GaAs/AlGaAs 2DEG samples below 0.5 K. *Surf. Sci.* **1996**, *361*, 537–541. [[CrossRef](#)]
21. Beenakker, C.; van Houten, H. Quantum transport in semiconductor nanostructures. In *Solid State Physics*; Academic Press: Cambridge, MA, USA, 1991; Volume 44, pp. 1–228.
22. Maradan, D.; Casparis, L.; Liu, T.M.; Biesinger, D.E.F.; Scheller, C.P.; Zumbühl, D.M.; Zimmerman, J.D.; Gossard, A.C. GaAs Quantum Dot Thermometry Using Direct Transport and Charge Sensing. *J. Low Temp. Phys.* **2014**, *175*, 784–798. [[CrossRef](#)]
23. Topinka, M.; LeRoy, B.; Westervelt, R.; Shaw, S.; Fleischmann, R.; Heller, E.; Maranowski, K.; Gossard, A. Coherent branched flow in a two-dimensional electron gas. *Nature* **2001**, *410*, 183–186. [[CrossRef](#)] [[PubMed](#)]
24. Rosen, I.T.; Andersen, M.P.; Rodenbach, L.K.; Tai, L.; Zhang, P.; Wang, K.L.; Kastner, M.; Goldhaber-Gordon, D. Measured potential profile in a quantum anomalous Hall system suggests bulk-dominated current flow. *arXiv* **2021**, arXiv:2112.13123.
25. Mukhopadhyay, U.; Dehollain, J.P.; Reichl, C.; Wegscheider, W.; Vandersypen, L.M.K. A 2 × 2 quantum dot array with controllable inter-dot tunnel couplings. *Appl. Phys. Lett.* **2018**, *112*, 183505. [[CrossRef](#)]
26. Dehollain, J.P.; Mukhopadhyay, U.; Michal, V.P.; Wang, Y.; Wunsch, B.; Reichl, C.; Wegscheider, W.; Rudner, M.S.; Demler, E.; Vandersypen, L.M.K. Nagaoka ferromagnetism observed in a quantum dot plaquette. *Nature* **2020**, *579*, 528–533. [[CrossRef](#)] [[PubMed](#)]